Corrosion Science 158 (2019) 108090

Contents lists available at ScienceDirect

Corrosion Science

journal homepage: www.elsevier.com/locate/corsci

Copper enriched by dealloying as external cathode in intergranular corrosion of aluminium alloy AA6005

Shilpa Kumari[a,1], Sigurd Wenner[b], John Charles Walmsley[b,c,2], Otto Lunder[a,b], Kemal Nisancioglu[a,*]

[a] Department of Materials Science and Engineering, Norwegian University of Science and Technology, N-7491 Trondheim, Norway
[b] SINTEF Industry, N-7465 Trondheim, Norway
[c] Department of Physics, Norwegian University of Science and Technology, N-7491 Trondheim, Norway

ARTICLE INFO

Keywords:
Microstructure
Electrochemistry
Segregation
Grain boundary
Intermetallics

ABSTRACT

The purpose of this work is to understand the role of Cu in the propagation mechanism of IGC on extruded alloy AA6005-T5. The constituent Cu segregates as a Cu-rich nanolayer, together with the formation of a solute depleted zone, along the grain boundaries during thermomechanical processing of the alloy. While the α-phase particles corrode in acidified chloride test solution, additional Cu becomes enriched as nanoscale particles and layer segments by dealloying on the external surface and fissure walls formed by IGC. While the grain-boundary layer functions as the internal cathode, enriched Cu acts as effective external cathodes in IGC propagation.

1. Introduction

The 6xxx-series is an important class of medium-strength Al alloys, based on the AlMgSi(Cu) system with good strength-to-weight ratio, formability, weldability and corrosion resistance [1,2]. However, unfavourable alloying and thermomechanical processing [2,3] have been shown to cause susceptibility to intergranular corrosion (IGC), especially in the presence of Cu [4] and/or Si in excess of the stoichiometric ratio for the equilibrium phase Mg_2Si [5]. Recent work has shown that Cu content in trace amounts (as low as 0.14 wt%) can cause susceptibility, depending on the temper and the type and amount of other alloying elements [6]. The susceptibility has been related to the segregation of a copper-rich layer with the thickness of a fraction of a monolayer along the grain boundaries (GBs) and a solute depleted zone adjacent to it, giving rise to microgalvanic coupling as the local driving force for IGC [6–12]. It has been claimed also that the α-Al(Fe,Mn,Cu)Si phase particles were important as the external cathodes during the initiation phase, losing their significance as they corroded away in the acidified chloride solution [13]. The role of the AlMgSiCu (Q) phase could not be clarified since it appeared to be inert during the initiation phase, based on characterization by scanning electron microscopy (SEM).

In recent related work [14], Cu was shown to become enriched at the surface of the corroding α-phase particles due to dealloying of the more active Al, Fe and Mn components in acidified chloride solution. However, the remaining Cu in the form of a debris of Cu flakes did not continue to function as the external cathodes because of poor contact with the underlying Al matrix. It was also found that different surface pre-treatment, such as mechanical polishing, Ar sputtering and alkaline etching, did not lead to significantly different initiation of IGC. By comparison, the as-received surface was initially protected against IGC by a crystalline oxide (mixture of γ- Al_2O_3, spinel $MgAl_2O_4$ and SiO_2), which was formed during extrusion and had a higher passivity than the air-formed film. Additional protection was provided also by partial coverage of the cathodic α-particles by smearing of the solid solution matrix alloy during extrusion.

The purpose of this paper is to investigate the significance of small Cu content on the formation of local cathodes and their function in determining the IGC propagation mechanism of alloy AA6005-T5 in acidified chloride solution. Corrosion testing is restricted to immersion in acidified chloride solution, in view of its practical significance in general and relevance to our earlier work in particular [6–9,12–14].

* Corresponding author.
E-mail address: kemaln@material.ntnu.no (K. Nisancioglu).
[1] Present address: Hydro Extruded Solutions, S-612 81 Finspång, Sweden.
[2] Present address: Department of Materials Science and Metallurgy, Cambridge University, CB3 0FS Cambridge, UK.

https://doi.org/10.1016/j.corsci.2019.07.014
Received 9 May 2019; Received in revised form 2 July 2019; Accepted 7 July 2019
Available online 09 July 2019
0010-938X/ © 2019 Elsevier Ltd. All rights reserved.

2. Experimental

2.1. Materials

The material focus was on extruded Al alloy AA6005-T5 (provided by Hydro), as described in our earlier work [6–9,12,13]. In summary, the billets were homogenized by heating from room temperature to 585 °C in 6.5 h and held at that temperature for 2.5 h. The billets were then air cooled and extruded to 4 mm thick and 150 mm wide plate-shape profiles. The profiles were cooled in a water spray cooling unit placed 2.5 m from the die exit, and stored for 2 h at room temperature before ageing for 5 h at 185 °C. The chemical composition of the alloy in wt%, as determined by spark optical emission spectroscopy, was 0.64% Si, 0.21% Fe, 0.14% Cu, 0.16% Mn and 0.56% Mg.

2.2. Corrosion test

The plate samples were masked with beeswax to expose an area of 20 × 20 mm^2 at each surface for the corrosion test (i.e., 800 mm^2 total). The cut edges of metal were not exposed. The samples were tested in the as-received condition without any pretreatment other than degreasing. Accelerated corrosion testing was based on the standard BS ISO 11846 method B, with modifications for the present purposes. Thus the test procedure involved immersion in acidified chloride solution, consisting of 30 g NaCl and 10 ml concentrated HCl (density = 1.19 g/ml) per liter of water, adjusted to pH 0.95 at room temperature. The test duration varied in the range 1.5–24 h in order to investigate the effect of exposure time on the corrosion morphology.

2.3. Electrochemical characterization

The open-circuit potential (OCP) was measured continuously during a corrosion test. Selected samples were rinsed and dried after the corrosion test and mounted on special holders exposing an area of 1 cm^2 before immersion in fresh acidified chloride solution for potentiodynamic polarization tests. In this respect, the polarization data are not exactly representative of precorroded surfaces. However, they were deemed sufficient for qualitative comparison of cathodic behaviour resulting from precorrosion. These tests were performed by using a DC 105 Gamry potentiostat. A conventional three electrode electrochemical cell was used. Separate specimens were used for anodic and cathodic polarization tests, which were performed at a scan rate of 0.5 mV/s starting from the OCP. At least three replicate measurements were performed for each type of sample.

2.4. Surface characterization

Glow discharge optical emission spectroscopy (GD-OES) was performed for depth-profiling on as-received and corroded samples. The GD-OES instrument used was a radio-frequency (RF) GD-PROFILER 2 supplied by HORIBA Jobin Yvon. Samples were sputtered in an argon atmosphere of 600 Pa and 32 W power with an anode diameter of 4 mm. The pressure and power specifications given above were the optimal values for the present purposes to obtain flat craters during Ar sputtering. The measurements were made every 5 ms during sputtering. The flatness of the crater bottoms was checked by use of a profilometer. The measurements were quantified for elements present in AA6005 alloy by using certified standards suitable for this particular alloy. However, the measurements, with an estimated error of 10% for replicate specimens, can at best be considered as semi-quantitative. The error results from the roughness of the original surface, limited reproducibility of the analyzed crater geometry and reliability of the standards.

The following types of surfaces were prepared for scanning electron microscope (SEM) characterization of corroded surfaces:

1 *As-tested surfaces for plan view of corrosion attack:* No further preparation was used after the corrosion test.
2 *Cross-sectional view of the IGC path:* Samples were cast in epoxy, followed by cutting and polishing the exposed cross section with colloidal silica, and finally the epoxy was broken off.
3 *Investigating the inner surfaces of the IGC fissures:* Samples were machined into standard tensile testing geometry first and then corroded in the standard acidified chloride test solution. The corroded samples were then strained to fracture by using a conventional tensile test instrument. In this manner the grain walls of the IGC fissures became clearly separated.

SEM imaging was performed in the secondary electron mode, using a Hitachi SU6600 and a Zeiss Ultra (model no 55 V P), both field emission gun (FEG) microscopes.

For investigating the chemistry of the near surface and corroded GBs, specimens for the transmission electron microscope (TEM) were prepared from 24 h corroded samples. These were first prepared according to one of the three types of procedures listed above. Cross-sectional TEM foils for investigating the external and IGC-fissure walls were prepared by using the conventional focused ion beam (FIB) lift-out procedure [15] in a FEI Helios G2 DualBeam FIB/SEM system.

TEM and scanning transmission electron microscope (STEM) observations were recorded on a JEOL JEM ARM200 F double corrected cold FEG microscope operating at 200 kV. Beam convergence angle of 34 mrad, beam current of 170 pA and expected probe size of 0.1 nm were used. A GIF Quantum spectrometer and a Centurio silicon drift detector were used for simultaneous mapping of electron energy loss spectroscopy (EELS) and energy-dispersive X-ray spectra (EDS), respectively. The EELS collection angle was 67 mrad, and the dispersion was 0.5 eV/channel, with 2x spectrum binning, allowing fast EELS acquisition with adequate energy resolution. Spatial mapping with EELS was performed by power-law background subtraction and integration of the Cu-L, O-K and C-K core loss edges [16]. EDS maps were obtained by integrating characteristic Kα peaks.

3. Results

3.1. Microstructure and corrosion morphology

Grain structure of alloy AA6005-T5 is shown in cross section in Fig. 1. The alloy appears to be fully recrystallized, with larger grains at and near the surface. Fig. 2 shows SEM image of a sample sectioned after corrosion for 24 h in the acidified test solution. The horizontal polished surface is the cross section, while the vertical surface was exposed to the test solution. Significant IGC was observed over the

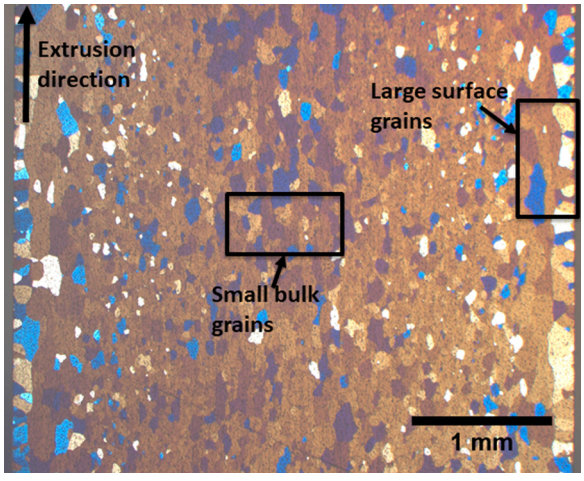

Fig. 1. Cross-sectional optical micrograph of AA6005 extruded alloy.

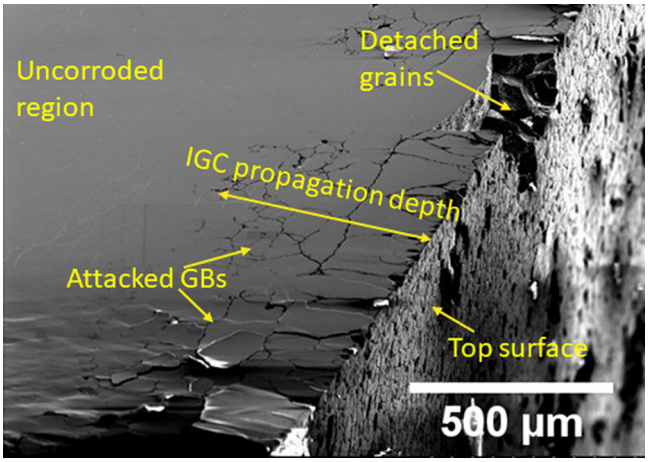

Fig. 2. Cross-sectional SEM image of sample near the surface, corroded for 24 h in acidified chloride solution.

entire exposed surface, attacking all exposed GBs down to an average depth of 150 µm from the surface, with the deepest attacks reaching to a depth of about 500 µm. Some grains, which lost contact with the adjacent grains due to IGC, were detached from the surface, probably during sectioning of the sample.

Fig. 3 shows typical plan view images of the corroded surface. The lower magnification image in Fig. 3a shows attacked GBs, filled with corrosion products, and grain surfaces which were etched by exposure to the test solution. The magnified area in Fig. 3b shows the micropitted morphology of the etched grain surface. Fig. 4a shows the attacked GB surface in an IGC fissure. The image of the area marked in Fig. 4a is magnified in Fig. 4b, showing the crystallographic-faceted etch surface commonly observed in localized corrosion forms of aluminium, such as tunnelling and pitting [17–19], due to significant acidification and Cl- enrichment of the anolyte. The etching probably occurred after the fissure was formed. It was not possible to document the tip morphology representative of propagation because of continuing etching after the specimen was removed from the test solution, despite rinsing. Nevertheless, the difference in the etch morphology between the interior grain-boundary walls (Fig. 4a and b) and the exterior grain surfaces (Fig. 3a and b) indicates that the pH was significantly lower in the anolyte than in the bulk test solution, as expected [20].

3.2. Electrochemistry

Fig. 5 shows the OCP of the AA6005 alloy as a function of exposure time in the acidified chloride solution. The decrease in the potential to a minimum at the outset is presumably related to breakdown of the protective oxide film [21]. The OCP showed monotonic increase after 2 h of exposure, indicating an ennobling-type process increasing with the time of exposure.

Fig. 6 shows potentiodynamic polarization curves for the as-received surface and surfaces which were corroded for different periods of time in the acidified chloride solution. Polarization tests were performed at a later stage, after the specimens were rinsed, dried and stored following the corrosion test and, therefore, do not represent the *in-situ* corrosion conditions. The cathodic and anodic parts of the curves, which were measured on different samples, are shown separately in Fig. 6a and b, respectively. The anodic curves were quite reproducible, nearly falling on top of each other for the three replicate samples for each corrosion condition specified on the figure. The curves shown are for a selected replicate for each condition. In contrast, significant increase in the cathodic activity was observed with increasing time of corrosion. The smallest current density observed on the as-received surface was due to the passivity of the surface caused by the protective thermal oxide formed during extrusion. The increase was small after 1.5 h of corrosion, which corresponded to the initiation phase, as can be inferred from the evolution of the OCP in Fig. 5. This indicates that the protective oxide was still present, maintaining the passivity of the surface. The cathodic current density increased by an order of magnitude after corrosion for 5 h, indicating significant cathodic activation by removal of the passivating oxide. The increase from 5 to 24 h exposure was again relatively small, although up to 100%.

3.3. GD-OES

GD-OES depth profile for O in Fig. 7a shows that the O concentration near the surface was significantly higher for the as-received samples and those exposed for 1.5 h to the acidified chloride solution, than the samples, which were exposed for 5 and 10 h. The profiles for Al in Fig. 7b show the opposite trend for corresponding exposure times, i.e., lower for the as-received and 1.5 h exposed samples, and higher for the 5 and 10 h exposed samples. These differences are attributed to the presence of the protective thermal oxide, which was formed during the extrusion of the samples, on the as-received and 1.5 h exposed cases [22]. The decrease in the O concentration and the corresponding increase in the Al concentration very near the surface indicates that 1.5 h of exposure to the acidified chloride solution started to dissolve the thermal oxide. Longer exposure was required for complete removal of the thermal oxide and its replacement by an air-formed oxide film as indicated by the profiles of 5 and 10 h corroded surfaces. These results are in agreement with the electrochemical polarization results of § 3.2. It should be recalled that the thickness of the thermal oxide is about 10 nm, as determined by TEM in the earlier, related paper [14]. The thickness indicated by the GD-OES profile for O on the as-received sample is somewhat thicker.

Fig. 7c indicates no significant change (perhaps a slight increase for the 1.5 h corroded surface) in the Cu concentration relative to the bulk value on the as-received and 1.5 h corroded surfaces covered by the

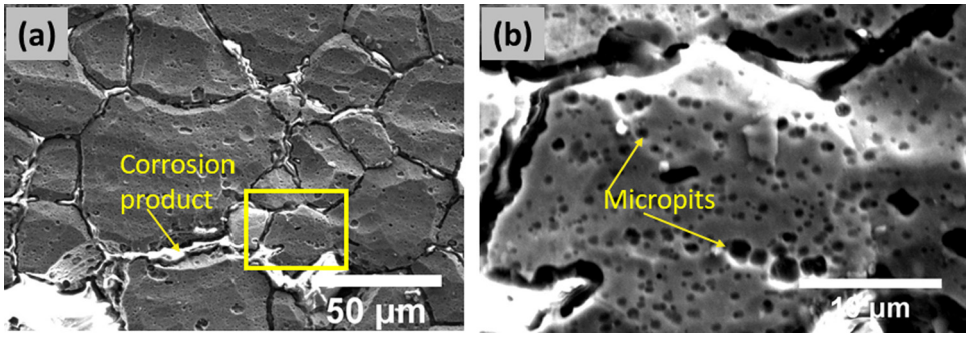

Fig. 3. (a) SEM image of surface corroded for 24 h, covered with micropits. (b) Area marked with a yellow square in (a) at a higher magnification, showing the micropits on the surface grains.

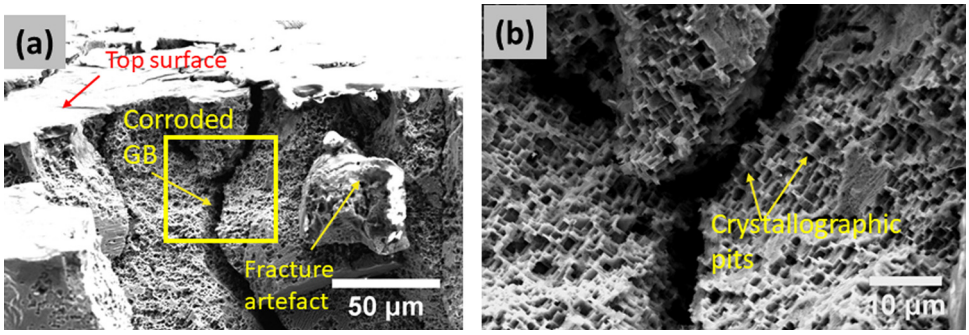

Fig. 4. (a) SEM image of IGC-attacked GB walls opened up by applying tensile stress perpendicular to the direction of filament propagation, showing crystallographic faceted attack. (b) Area marked with yellow square in (a) at a higher magnification.

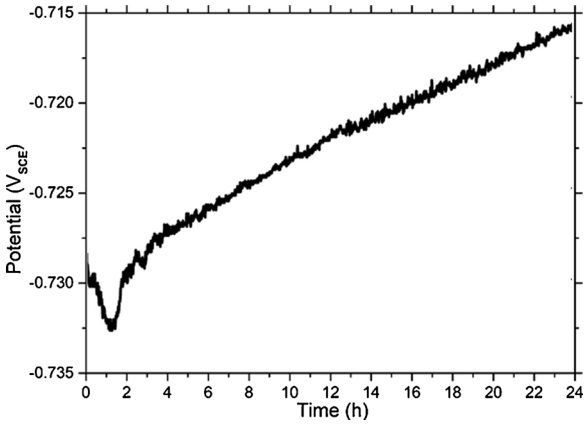

Fig. 5. OCP versus exposure time for as-received AA6005 alloy in acidified chloride solution.

thermally formed oxide. A significant increase in the Cu concentration at the surface with increasing exposure time in acidified chloride solution is observed, indicating that the above-mentioned changes in the cathodic behaviour must be due to enrichment of Cu on the surface by dealloying of aluminium during exposure to the test solution. The uncorroded (as-received) samples show significant Mg (Fig. 7d) and Si (Fig. 7e) enrichment at the surface. This is related to the enrichment of the oxides of the two elements in the mixed thermal oxide formed by extrusion [14,22]. The enrichment is confined to a 10 nm thickness for Mg, corresponding to the TEM value of the thermally-formed oxide thickness. However, the O and Si profiles for the as-received sample persist up to about 20 nm below the surface. It is evident from Fig. 7d that enriched Mg is removed by exposure to the acidified chloride test solution, and Si is significantly reduced (Fig. 7e). A small enrichment of Si still appears to remain on the corroded surface.

The source of Fe and Mn in the profiles shown in Fig. 7f and g, respectively, is the α-phase particles. The decrease of the profiles toward the as-received surface (the black squares in Fig. 7f and g, respectively) is attributed to smearing of Al metal over the α-phase particles during extrusion [14,22]. Fe and Mn concentrations increase with depth toward their respective bulk values as the smeared layer is removed by Ar sputtering. Similar decrease of the Fe and Mn profiles toward the surface for the 5 and 10 h corroded samples is attributed to the corrosion of the α-particles in the acidified chloride solution [13,14]. These profiles also increase with increasing depth toward their bulk values as uncorroded α-phase particles become exposed by Ar sputtering. In summary, the GD-OES results show that the only constituent element becoming enriched at the surface by corrosion in the acidified chloride solution is Cu, thus becoming the dominating external cathode.

3.4. TEM analysis

The nature of Cu segregation by dealloying of the exposed surface and the corrosion morphology inside the IGC filaments were investigated further by use of STEM, EDS and EELS analyses of cross-sectional foils of corroded areas near the surface. Fig. 8a is a cross-sectional annular dark-field (ADF) STEM image of a 24 h corroded surface showing the metal matrix-oxide interface and a corroded GB. The bright particles in the bulk of Fig. 8a are α-Al(FeMnCu)Si phases. The areas marked with yellow and red rectangles in Fig. 8a are shown at higher magnifications in Fig. 8b and e, respectively. Fig. 8c and f show EELS elemental maps of Fig. 8b and e, respectively, identifying the bright features as Cu. It is thus evident that Cu was segregated both as Cu-rich nanolayer segments at the metal-oxide interface (Fig. 8e and

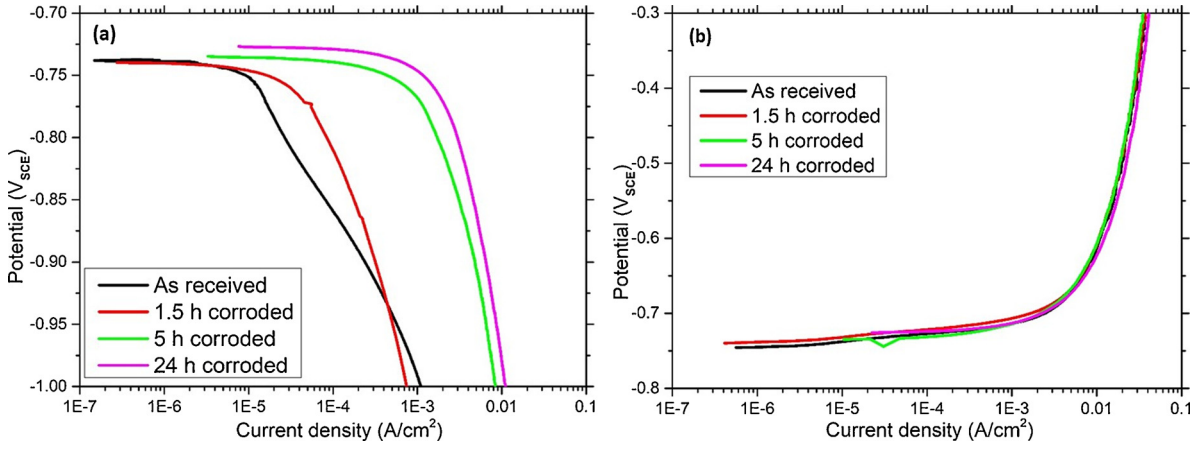

Fig. 6. (a) Cathodic and (b) anodic polarization curves for AA6005 alloy after various periods of corrosion in acidified chloride solution at 25 °C.

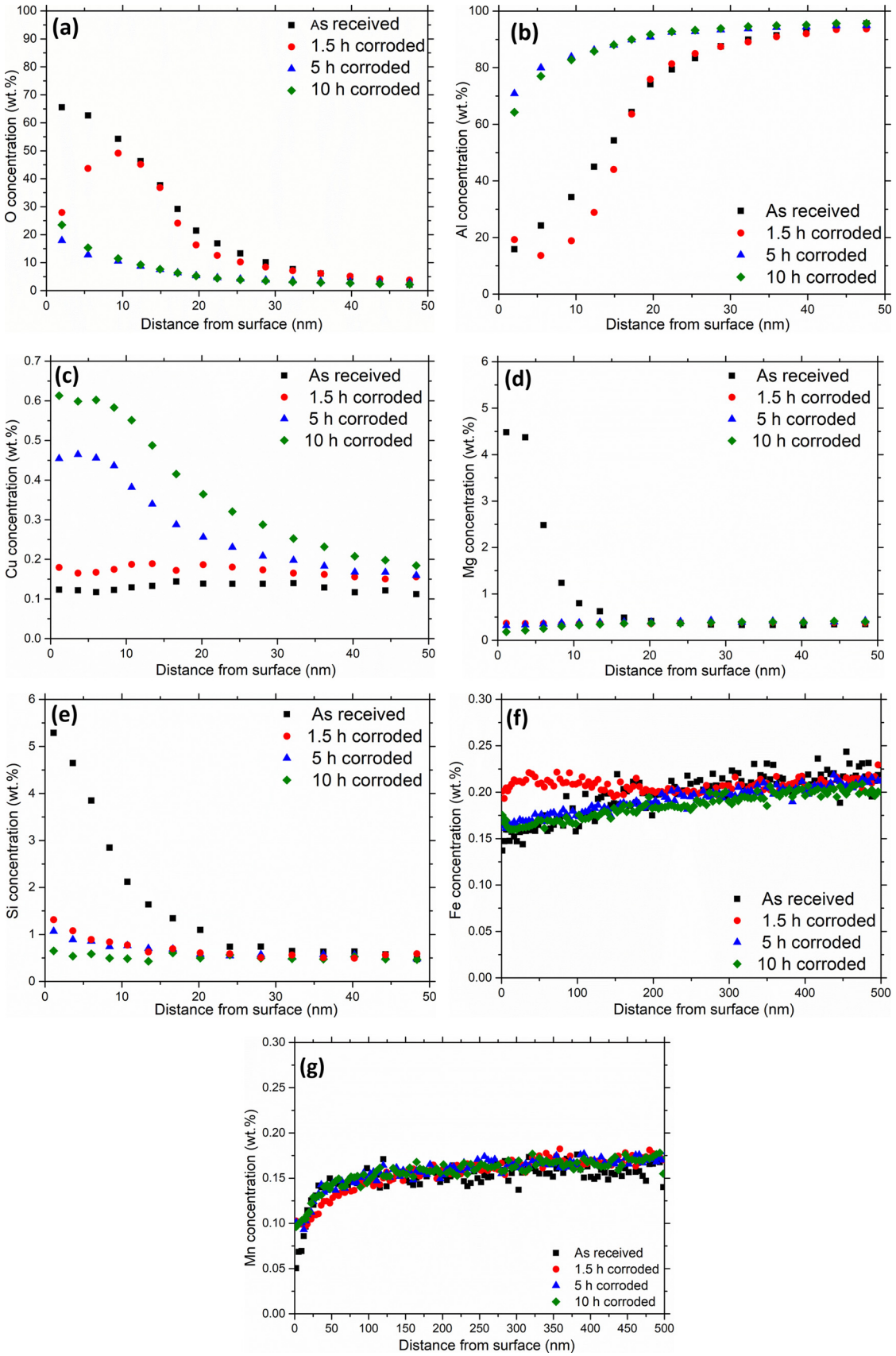

Fig. 7. GD-OES elemental depth profiles of (a) O, (b) Al, (c) Cu, (d) Mg, (e) Si, (f) Fe and (g) Mn for as-received and corroded samples.

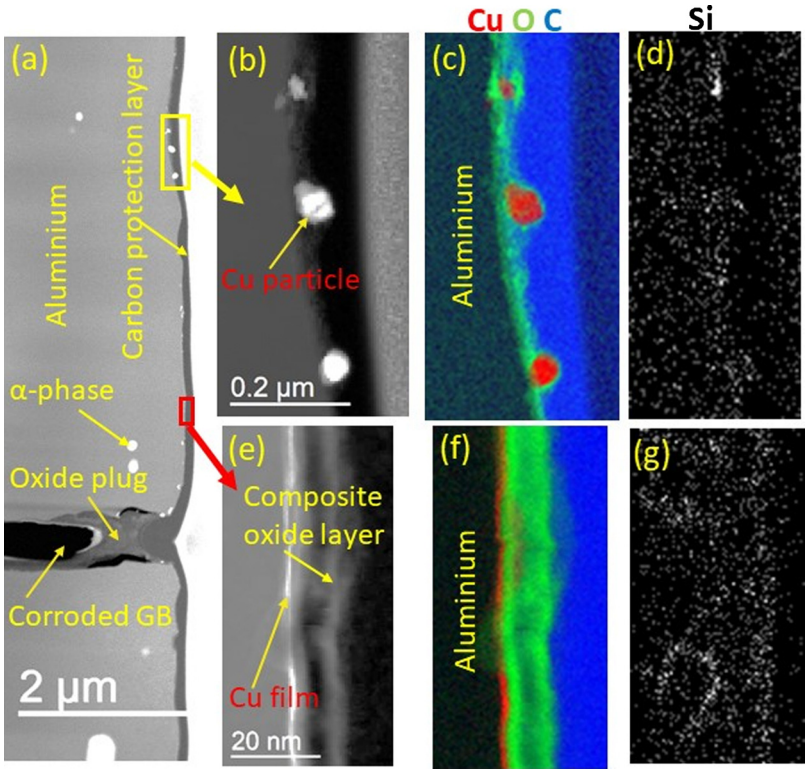

Fig. 8. (a) Annular dark-field (ADF) STEM image of a cross section near the top surface of AA6005 sample after 24 h corrosion in acidified chloride solution. (b) ADF STEM image of the yellow rectangle in image (a) showing Cu particles at the matrix-oxide interface. (c) EELS map of image (b) where the areas coloured red, green and blue correspond to Cu, O and C, respectively. (d) EDS map of Si corresponding to image (b). (e) ADF STEM image of the red rectangle in (a) showing a 1–2 nm thick discontinuous metallic Cu-rich layer. (f) EELS map of image (e). (g) EDS map of Si corresponding to image (e).

f) and as discrete particles embedded in the oxide (Fig. 8b and c). The Cu particles in Fig. 8b are about 50 nm in size. Many of these were detached from the underlying Al-alloy matrix, while the Cu-rich layer segments were located along the metal matrix-aluminium oxide interface, apparently in contact with the Al matrix. The segments were about a few hundred nm in length. Similar results from investigation of several foils are summarized in Ref. [22]. EDS analysis of Si at the same location, shown in Fig. 8d, indicates the presence of Si associated with a small fraction of the Cu particles, such as the top particle in Fig. 8b and c, while Fig. 8g suggests that there was no Si associated with the Cu-rich layer. These results indicate that the Cu-rich layer segments formed by dealloying of the aluminium matrix are expected to act as the external cathodes, while the Cu-rich particles, probably formed by dealloying of the α-phase particles, but without contact with the underlying matrix, do not have a similar function, as discussed in §1.

The fissures formed by IGC were filled with corrosion products, as indicated by the corroded GB morphology in Fig. 3a and the oxide plug at the fissure opening in Fig. 8a. Some of these products were probably removed mechanically and/or chemically during specimen preparation. As earlier studies indicate, the width of GB attack was much smaller at the tip of the fissure than those images presented here, probably confined to the width of the solute depleted zone [9]. The tail of the fissure broadened as a result of creep and continuing corrosion on the walls, which resulted in the morphology shown in Fig. 8a.

The cross-sectional oxide morphology on the Cu-rich layer, observed in Fig. 8e and 8f, indicates the presence of a composite oxide layer, consisting of a hydrated outer layer, probably formed during IGC, and an inner layer, probably formed during exposure of the sample to ambient atmosphere after the IGC test and during preparation of the TEM foil.

EDS analysis of the corroded grain surface a bit deeper in the same fissure, within the area marked by a rectangle in Fig. 9a at a higher magnification (Fig. 9b), indicated the presence of a Cu-rich layer at the metal-oxide interface (Fig. 9d), similar to that discussed in connection with Fig. 8e. It was probably formed by dealloying during broadening of the fissure tail by corrosion. Formation of a composite oxide is indicated by the EDS images for Al and O in Fig. 9c and e, respectively, in correspondence with the EELS images in Fig. 8e and 8f.

A SEM image of the IGC attacked fissure surface in a GB, obtained by tensile separation along the GB, is shown in Fig. 10. A TEM specimen was prepared by using the FIB lift-out technique, as shown in the figure, from about 65 μm depth below the exposed fissure wall. ADF STEM image of this specimen is shown in Fig. 11a. Fig. 11b and e are the magnified images of the two marked areas in Fig. 11a, showing bright particles embedded in the aluminium oxide covering the corroded GB. Fig. 11c and f show EELS analyses for Fig. 11b and e, respectively, indicating that the particles are Cu rich. In contrast to Fig. 9, which represents a corroded GB close to the sample surface, no Cu-rich layer or its remnants could be detected at the present depth inside the IGC fissure. The EDS maps in Fig. 11d and g show that Si remnants seem to be present in the oxide. This is probably analogous to the remnants of Si detected at the surface of corroded samples in Ref. [14,22], which was interpreted as Si formed by dealloying and existing in its stable form SiO_2 in the surface oxide or corrosion products.

4. Discussion

The present work gives new evidence about the roles of external and internal cathodes in IGC of aluminium alloy AA6005. Earlier work showed that external cathodes, thought to consist mainly of α-phase particles, corroded away in acidified chloride solution. Hence, the dominant cause for IGC corrosion was suggested to be due to internal cathodes in the form of a segregated Cu-rich nanolayer along the GBs [9,12]. The present results suggest that Cu becomes enriched also on the exposed external surface and corroded GB walls in the fissures formed by IGC, as a result of dealloying in the presence of the acidified chloride solution. Cu is the only enriched element, since it is thermodynamically immune to corrosion at the potentials observed during corrosion, while the other constituents of the material, Fe, Mn, Mg and Si, are active [23]. Although fresh α-phase particles become exposed, this process is delayed since a certain thickness, commensurate with the distance between the particles, of the alloy matrix has to corrode, both

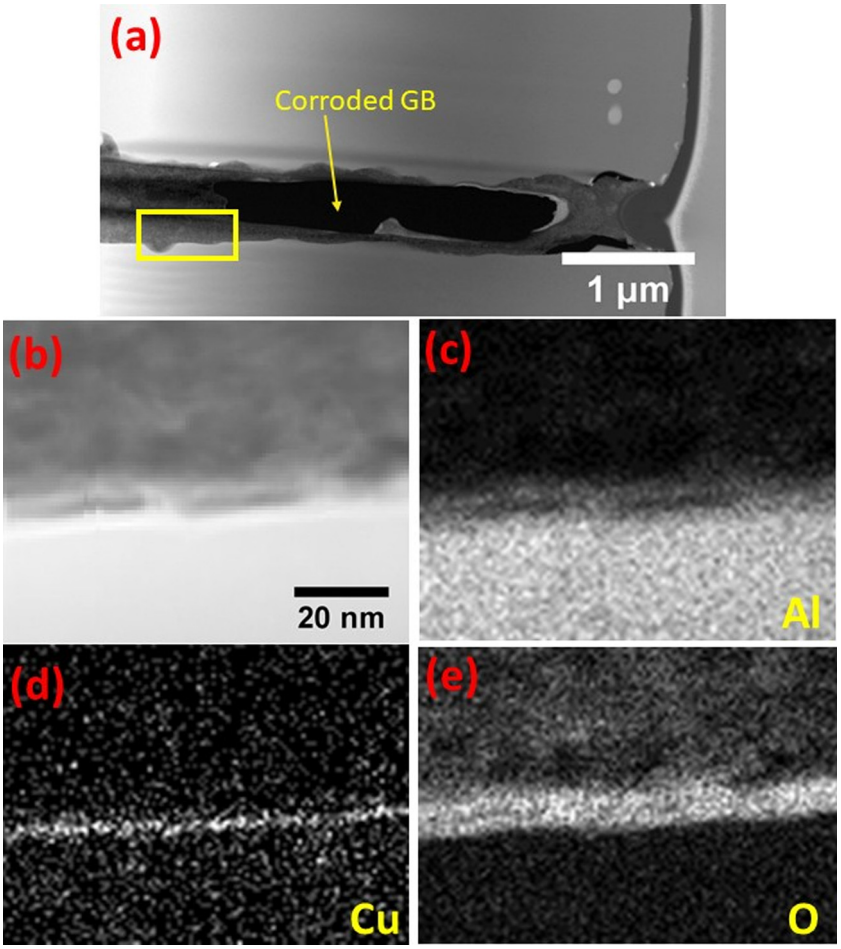

Fig. 9. (a) Visualization of a deeper location in the fissure shown in Fig. 8a. (b) ADF STEM image of the yellow rectangle in image (a). EDS maps of the area in (b) for (c) Al, (d) Cu and (e) O.

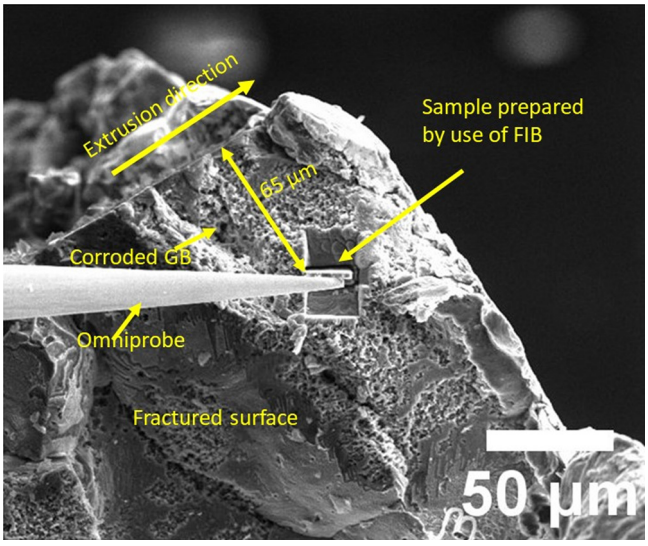

Fig. 10. SEM image of fractured surface showing the location where TEM specimen was obtained by use of the FIB preparation technique. The milled sample is in the process of being lifted out by use of a tungsten lift-out needle. The arrow labelled "Extrusion direction" lies parallel to the top surface exposed to the test solution.

in the IGC filaments and the outer surface, while Cu is continuously refreshed at both locations at a faster rate by dealloying.

Copper enrichment of the surface due to corrosion in the acidified chloride solution is indicated by all *ex-situ* analytical tests used in this work, including GD-OES, STEM EELS/EDS and cathodic polarisation. Lack of an appreciable effect of acid corrosion on the anodic polarization curves may be an artefact of exposing the samples to ambient air before the polarisation test, e.g., due to passivation of the corroded sites. However, the kinetics of anodic oxidation (pitting) is probably determined more by the bulk than the surface properties of the aluminium alloy and, therefore, not much affected by enrichment of Cu present at the low level in the bulk material. The effect of precorrosion in the acidified chloride solution on the electrochemical behaviour of these specimens deserves further work. Based on the data obtained, however, the change in the OCP with the time of exposure to the acidified chloride solution (Fig. 5) can be tentatively attributed to increase in the cathodic area, rather than direct ennoblement of the anodic breakdown potential of the surface, by Cu enrichment due to dealloying.

The present work shows that Cu is enriched in the form of a few nm thick layer segments at the metal-oxide interface along the exterior and interior surfaces. Cu-rich segments were also observed, although fewer, along the corroded fissure walls. These could be the remnants of the original GB layer, segregated during thermomechanical processing of the samples. 30–50 nm size Cu-rich particles were more common deeper in the filaments. Cu particles were observed also on the external surface, mostly embedded in the oxide layer and, therefore, detached from the metal matrix. These particles are believed to be mainly the

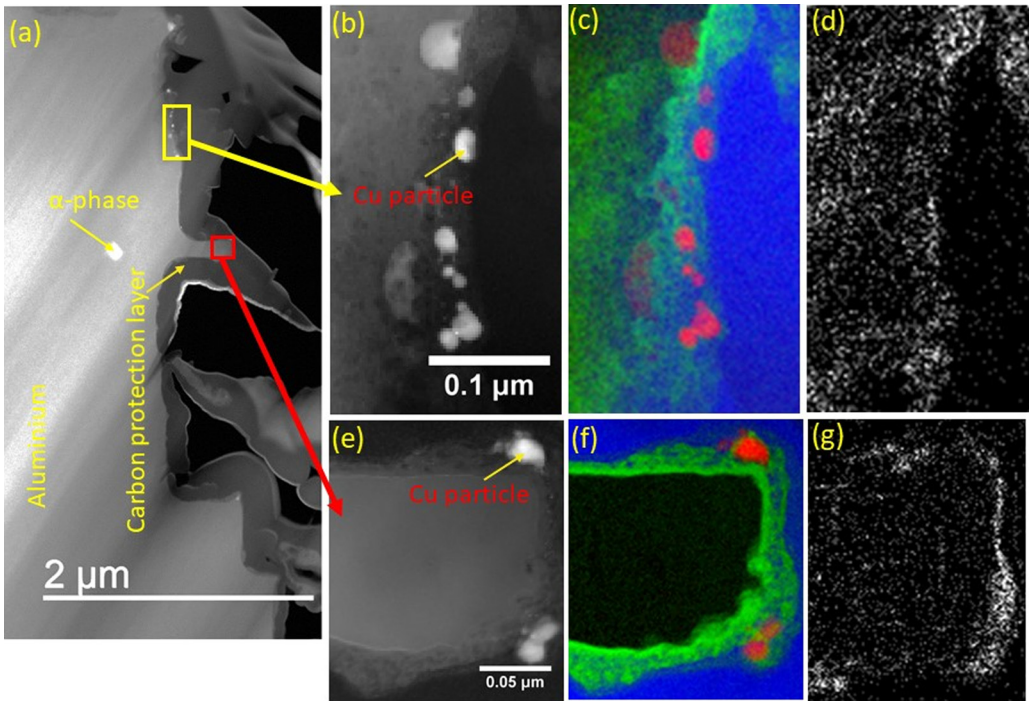

Fig. 11. (a) ADF STEM image near a corroded GB on the fractured fissure wall of an AA6005 sample after 24 h corrosion in acidified chloride solution. (b) ADF STEM image of yellow rectangle in image (a) showing, at higher magnification, Cu particles at the matrix-oxide interface. (c) EELS map of image (b). (d) EDS Si map of image (b). (e) ADF STEM image of red rectangle in (a). (f) EELS map of image (e). (g) EDS Si map of image (e).

remnants of dealloyed α-phase particles. They can also form by coarsening of the Cu-rich layer, formed by dealloying during exposure to the test solution, as the layer becomes detached from the metal surface during corrosion.

The morphological dissimilarities indicate that the chemistry of the corroding external and internal surfaces is different. The dense crystallographic faceted etching internally, as opposed to the smaller density of micropits externally, indicate the formation of a considerably more acidic chloride environment internally in relation to the external environment. The bulk solution is initially already acidic at pH 0.95. However, the pH in the bulk solution is expected to increase appreciably during the corrosion test [24]. Existence of a more acidic anolyte in the fissures is possible only with significant participation of the external cathodes in the corrosion process. The fundamental electrochemical principle of separation of the catholyte and anolyte in localized metal corrosion is thus satisfied. With the foregoing information at hand, the earlier sketch [9] for the mechanism of IGC on 6xxx Al alloys with small Cu content can be modified to that shown in Fig. 12.

The present study lacks chemical and morphological data for the IGC fissure tip, where the rate of penetration of the IGC fissures into the material is determined. The GB Cu-rich layer as the internal cathode and the solute depleted zone as the anode are still believed to be the dominating factors determining the propagation mechanism, probably to increasing extent as the IGC attack propagates deeper. The role of the Cu-rich nanolayer along the GBs is still deemed crucial in the propagation mechanism because breaking of the continuity by coarsening of the layer into precursors of the Q-phase by aging increases the IGC resistance [8,9]. However, the present characterization results are limited to the morphology of the tail, where the corrosion mechanism must be very similar to that of acid etching of bulk aluminium in acidified chloride solution forming the observed crystallographic etch morphology at a later stage in the propagation process [17].

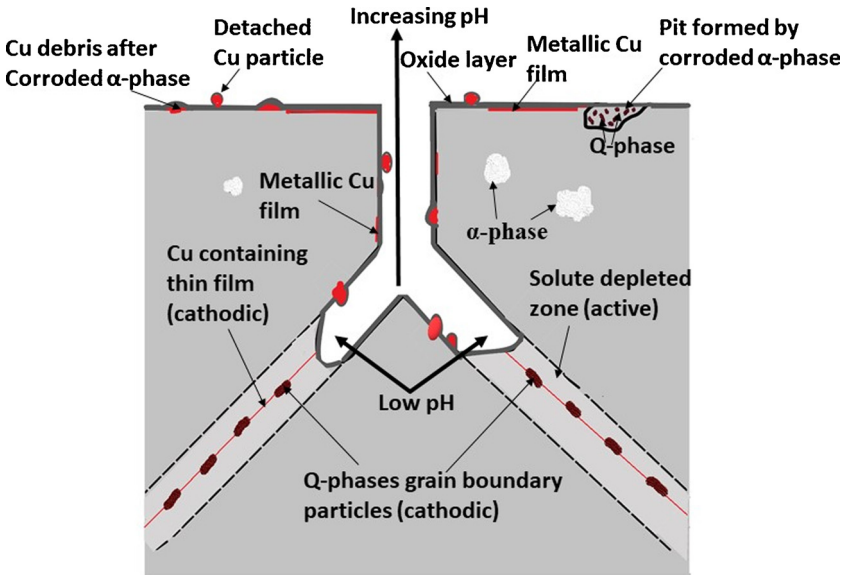

Fig. 12. Conceptual sketch of the IGC mechanism in Cu-containing 6xxx alloys.

5. Conclusions

1 The cathodic activity during IGC propagation on the AA6005 alloy with small Cu content increases with the time of immersion in acidified chloride solution. This is caused by enrichment of Cu in the propagating IGC filaments and on the outer surface as a result of dealloying.
2 Initially, the α-phase and the Cu-rich nanolayer along the GBs are the external and internal cathodes, respectively, in driving the IGC process. The α-phase corrodes, and exposure of a fresh α-phase particle is delayed because of the distance between the particles in the alloy. Meanwhile, Cu enriches continuously by dealloying at the corroding sites and becomes the dominating cathode both externally and internally.
3 The difference in the etching morphology between the external surface and the IGC filaments suggests indirectly that the pH is lower, and the chloride concentration higher in the filaments than those in the bulk solution. This can occur only by participation of the external cathodes in the propagation of IGC. Thus, the principle of separation of the anodic and cathodic sites in localized corrosion is satisfied.

Data availability

The raw data required to reproduce these findings cannot be shared at this time from a permanent web link due to technical and time limitations. Please contact the first author at shilpa.kumari@hydro.com.

The processed data required to reproduce these findings are available to download from http://hdl.handle.net/11250/2584914.

Acknowledgements

This work was performed as part of the Norwegian national project entitled, *Fundamentals of Intergranular Corrosion in Aluminium Alloys (FICAL)*, supported by The Research Council of Norway (contract no. 247598), Hydro, Gränges, Benteler Automotive Raufoss, and Steertec Raufoss. The STEM work was performed under the auspices and infrastructure of the Norwegian Transmission Electron Microscopy Centre (NORTEM) supported by The Research Council of Norway, contract no. 197405.

References

[1] J.R. Davis, Corrosion of Aluminum and Aluminum Alloys, ASM International, Metals Park, OH, USA, 1999.
[2] L.F. Mondolfo, Aluminum Alloys: Structure and Properties, Butterworths, London, UK, 1976.
[3] J.E. Hatch, Aluminum Properties and Physical Metallurgy, ASM International, Metals Park, OH, USA, 1984.
[4] K. Yamaguchi, K. Tohma, Japan Inst. Light Metals 47 (1997) 285–291.
[5] A.K. Gupta, D.J. Lloyd, Mater. Sci. Eng. A 316 (2001) 11–17.
[6] G. Svenningsen, J.E. Lein, A. Bjørgum, J.H. Nordlien, Y. Yu, K. Nisancioglu, Corr. Sci. 48 (2006) 226–242.
[7] G. Svenningsen, M.H. Larsen, J.H. Nordlien, K. Nisancioglu, Corr. Sci. 48 (2006) 258–272.
[8] G. Svenningsen, M.H. Larsen, J.H. Nordlien, K. Nisancioglu, Corr. Sci. 48 (2006) 3969–3987.
[9] G. Svenningsen, M.H. Larsen, J.C. Walmsley, J.H. Nordlien, K. Nisancioglu, Corr. Sci. 48 (2006) 1528–1543.
[10] S.K. Kairy, T. Alam, P.A. Rometsch, C.H.J. Davies, R. Banerjee, N. Birbilis, Metall. Mater. Trans. A 47 (2016) 985–989.
[11] N. Birbilis, Y.M. Zhu, S.K. Kairy, M.A. Glenn, J.F. Nie, A.J. Morton, Y. Gonzalez-Garcia, H. Terryn, J.M.C. Mol, A.E. Hughes, Corr. Sci. 113 (2016) 160–171.
[12] M.H. Larsen, J.C. Walmsley, O. Lunder, K. Nisancioglu, J. Electrochem. Soc. 157 (2010) C61–C68.
[13] K. Shimizu, K. Nisancioglu, ECS Electrochem. Lett. 3 (2014) C29–C31.
[14] S. Kumari, S. Wenner, J.C. Walmsley, O. Lunder, K. Nisancioglu, J. Electrochem. Soc. 166 (2019) C3114–C3123, https://doi.org/10.1149/2.0211911jes.
[15] L.A. Giannuzzi, F.A. Stevie, Micron 30 (1999) 197–204.
[16] V.C. Angadi, C. Abhayaratne, T. Walther, J. Microsc. 262 (2016) 157–166.
[17] M. Baumgärtner, H. Kaesche, Corr. Sci. 29 (1989) 363–378.
[18] I.L. Muller, J.R. Galvele, Corr. Sci. 17 (1977) 179–193.
[19] V. Guillaumin, G. Mankowski, Corr. Sci. 42 (2000) 105–125.
[20] Z. Szklarska-Smialowska, Corr. Sci. 41 (1999) 1743–1767.
[21] H.H. Strehblow, Mater. Corros. 35 (1984) 437–448.
[22] S. Kumari, Initiation and Propagation of Intergranular Corrosion on AA6005 Aluminium Alloy, PhD Thesis, Norwegian University of Science and Technology, Trondheim, Norway, 2018http://hdl.handle.net/11250/2584914.
[23] M. Pourbaix, Atlas of Electrochemical Equilibria in Aqueous Solutions, National Association of Corrosion Engineers, Houston, TX, USA, 1974.
[24] D. Zander, C. Schnatterer, C. Altenbach, V. Chaineux, Mater. Design 83 (2015) 49–59.